Orientation-dependent stress relaxation in hetero-epitaxial 3C-SiC films

Francesca Iacopi, Glenn Walker, Li Wang, Laura Malesys, Shujun Ma, Benjamin V. Cunning, and Alan Iacopi

Citation: Appl. Phys. Lett. **102**, 011908 (2013); doi: 10.1063/1.4774087
View online: http://dx.doi.org/10.1063/1.4774087
View Table of Contents: http://aip.scitation.org/toc/apl/102/1
Published by the American Institute of Physics

Articles you may be interested in

Quantitative evaluation of biaxial strain in epitaxial 3C-SiC layers on Si(100) substrates by Raman spectroscopy
Journal of Applied Physics **91**, 1113 (2002); 10.1063/1.1427408

Epitaxial growth of 3C–SiC films on 4 in. diam (100) silicon wafers by atmospheric pressure chemical vapor deposition
Journal of Applied Physics **78**, 5136 (1998); 10.1063/1.359745

Production of large-area single-crystal wafers of cubic SiC for semiconductor devices
Applied Physics Letters **42**, 460 (1998); 10.1063/1.93970

Large-band-gap SiC, III-V nitride, and II-VI ZnSe-based semiconductor device technologies
Journal of Applied Physics **76**, 1363 (1998); 10.1063/1.358463

Stress relaxation during the growth of 3C–SiC / Si thin films
Applied Physics Letters **89**, 131906 (2006); 10.1063/1.2357569

Brittle dynamic fracture of crystalline cubic silicon carbide (3C-SiC) via molecular dynamics simulation
Journal of Applied Physics **98**, 103524 (2005); 10.1063/1.2135896

HIGH-VOLTAGE AMPLIFIERS AND ELECTROSTATIC VOLTMETERS

ENABLING RESEARCH AND INNOVATION IN DIELECTRICS, MICROFLUIDICS, MATERIALS, PLASMAS AND PIEZOS

APPLIED PHYSICS LETTERS 102, 011908 (2013)

Orientation-dependent stress relaxation in hetero-epitaxial 3C-SiC films

Francesca Iacopi,[1,a)] Glenn Walker,[1] Li Wang,[1] Laura Malesys,[2] Shujun Ma,[3] Benjamin V. Cunning,[1] and Alan Iacopi[1]
[1]*Queensland Micro and Nanotechnology Centre, Griffith University, Nathan, 4111 QLD, Australia*
[2]*Ecole d'Ingenieurs, Materiaux, Universite de Bourgogne, Dijon, France*
[3]*Mechanical Engineering Department, University of Queensland, St. Lucia, 4072 QLD, Australia*

(Received 22 August 2012; accepted 18 December 2012; published online 9 January 2013)

Residual stresses in epitaxial 3C-SiC films on silicon, for chosen growth conditions, appear determined by their growth orientation. Stress evaluation locally with Raman spectroscopy, and across a 150 mm wafer with curvature measurements, indicate that thin films can be grown on Si(100) with residual tensile stresses as low as 150 MPa. However, films on Si(111) retain a considerably higher stress, around 900 MPa, with only minor decrease versus film thickness. Stacking faults are indeed geometrically a less efficient relief mechanism for the biaxial strain of SiC films grown on Si(111) with ⟨111⟩ orientation. Residual stresses can be tuned by the epitaxial process temperatures. © *2013 American Institute of Physics*. [http://dx.doi.org/10.1063/1.4774087]

Mono- and poly-crystalline thin 3C-SiC films on silicon have been extensively explored over the last 10–15 years.[1,2] Such films hold excellent promise as material for micro-electro-mechanical systems (MEMS) thanks to the outstanding mechanical properties of SiC (second hardest material after diamond, with elastic modulus in the range 300 to 700 GPa, and high wear resistance[3]). Additionally, epitaxial SiC films on Si enable silicon micromachining techniques, making the whole MEMS fabrication process substantially easier and cheaper as compared to the use of bulk SiC substrates.[4,5]

Although poly-3C-SiC films are easier to grow on silicon, mono-crystalline SiC films are superior to in terms of fracture strength and therefore attract substantially more interest.[6] However, the typically high residual stresses generated upon the hetero-epitaxy (due to the mismatch of lattice and coefficient of thermal expansion between the Si and SiC, about 20% and 25%, respectively[3]) and the limited understanding of their relaxation mechanism have been so far a major limitation for the application of 3C-SiC films in the MEMS area.[4,5] Control and reproducibility of residual stress state in MEMS building blocks such as diaphragms and beams are critical as directly related to their performance (operating frequencies and sensing forces) and reliability (fracture strength).[4,7]

The limited understanding of residual stresses for 3C-SiC on Si and the presence of contradictory reports in the literature are due to the hurdles in obtaining a systematic and comprehensive stress analysis of the hetero-epitaxial films.[8–10] Raman spectroscopy has been the most common mean of stress analysis for 3C-SiC films,[11,12] however, the stress information from Raman is local, i.e., typically from a few μm^2 film area, and as it relates to an averaged stress for all fundamental directions.[13] A quantitative assessment of biaxial strain with Raman spectroscopy needs specific and accurately calibrated biaxial coefficients.[14] Sensitivity is also limited for very thin SiC films on Si substrates (below 100 nm), as silicon has a strong Raman response weakening the 3C-SiC transversal optical (TO) peak and completely masking the 3C-SiC longitudinal optical (LO) response around 972 cm^{-1},[15] as shown in Fig. 1.

On the other hand, stress analysis through the monitoring of wafer curvature yields information over the biaxial stress state of the whole epitaxial film and works well for very thin SiC films. However, the use of such method has been limited by the typically high non-uniformity of film thickness over large areas.[8] Zielinski *et al.*[10] have investigated kinetic factors in the relaxation of 3C-SiC films on Si(100) versus growth temperature, but they have not reported on the role of the starting Si surface plane and their work focused on relatively thick films (1–16 μm).

The recent availability of 3C-SiC epitaxial films with exceptional within wafer thickness uniformity (better than 1.5% (Ref. 16)) over areas up to 150 mm wafer diameter on both Si(100) and Si(111) surfaces has enabled a systematic study of residual stress state of films below 1 μm thickness, down to 60 nm, which are of high relevance for MEMS. Further relevance of this work is given by the fact that 3C-SiC

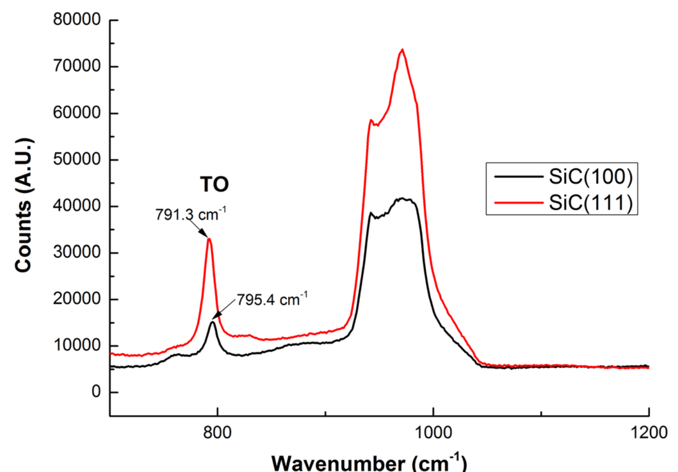

FIG. 1. Raman spectra showing the region around the TO and LO peaks for 1 μm thick SiC(100) and SiC(111) films. Both spectra show a red shift of the TO peaks as compared to unstressed 3C-SiC films, with TO peak at 796 cm^{-1}, indicating residual tensile stress.

a)Author to whom correspondence should be addressed. Electronic mail: f.iacopi@griffith.edu.au.

 © 2013 American Institute of Physics

on Si(111) is a potentially ideal template for the growth of III-nitrides on silicon, where the management residual stresses are fundamental to avoid extensive layer cracking.[17]

A deeper understanding of 3C-SiC strain relief mechanisms on the common Si(100) and Si(111) surfaces offers a key to the control of residual stresses in highly mismatched hetero-epitaxy and to the wider use of 3C-SiC films in MEMS either as a standalone or enabling other mismatched epitaxial processes on silicon.[18]

3C-SiC films were deposited at 1000 °C on on-axis 150 mm Si(100) and Si(111) wafers in a custom made hot-wall horizontal low-pressure chemical vapour deposition (LPCVD) system using a process with alternate supply of SiH_4 and carbon source gas similar to the one described by Wang *et al.*[16] Main differences are the use of C_3H_6 as carbon source and a carbonization process at 950 °C. Some epitaxial runs were performed either with a lower carbonisation temperature (750 °C) or a higher growth temperature (1050 °C), for comparison. Films were grown with thicknesses between 60 nm and 1.5 μm. Nanoindentation was performed on the 1 μm thick films with a Hysitron Triboindenter to retrieve the elastic modulus (E) of the 3C-SiC films.[19]

An InVia Renishaw Raman spectroscopy system with $\lambda = 514$ nm was used for monitoring Raman shifts of the TO SiC peak of the epitaxial films, using a laser spot size of about 1 μm diameter. The calibration was based on the 520.5 wavenumber Si mode, and measurements were taken on several positions across the 150 mm wafer. The local film stress was estimated using the shift coefficient for the TO peak calibrated by Rohmfeld *et al.*[14] for 3C-SiC films on Si(100) and the E value of 3C-SiC films as measured with nanoindentation.

A Tencor Flexus 2320 system was used for monitoring wafer curvature prior to and after epitaxial growth. The measurements were done along the diameter of 150 mm wafers with 10 mm edge exclusion. The biaxial stress for SiC films was calculated on the basis of the modified Stoney's equation,[20] using the appropriate elastic moduli (E) and Poisson's ratios (ν) values: 130 GPa and 170 GPa, 0.28 and 0.26 for Si(100) and Si(111), respectively.[21] Transmission electron microscopy (TEM) and low energy electron diffraction (LEED) analyses were performed with a FEI Tecnai F30 system. Additionally, X-ray diffraction (XRD) was performed systematically on the epitaxial films as control measurement for crystalline quality with a Bruker D8 Advance spectrometer (CuKα radiation).

Atomic force microscopy was performed on an NT-MDT NTEGRA spectra. Samples were imaged with dimensions of $5 \times 5\ \mu m^2$ in contact topography mode with NT-MDT CSG01 probes.

The Raman analysis yielded the presence of a residual tensile stress for all of the SiC films, indicated by a red shift with respect to the unstressed TO peak position for 3C-SiC at 796 cm^{-1}.[22] Typical Raman spectra from 1 μm thick films are shown in Fig. 1. The TO peak positions for SiC films on Si(100) showed a 0.6–1.2 cm^{-1} red shift. Using the coefficients calculated by Rohmfeld *et al.*[14] and E = 330 GPa from nanoindentation of SiC(100) films, a residual tensile stress between 180 and 360 MPa was calculated.

The TO peak positions for SiC films on Si(111) showed a 3–4.7 cm^{-1} red shift, and the same Raman coefficients combined to E = 400 GPa for SiC(111) films would lead to an estimate of residual tensile stress between 1.2 and 1.7 GPa. The variation of the TO peak position within wafer was less than 1 wavenumber for both film types. Also, note that films 100 nm thick and below did not yield a Raman signal strong enough to allow accurate analysis.

Fig. 2 shows the global film stress versus film thickness as calculated from wafer curvature data. The uncertainty on the stress values calculated with this method is within 10% variation. A linear regression is shown for both SiC on Si(100) and SiC on Si(111) series to guide the eye. The SiC films on Si(111) show a high residual stress, with average around 900 MPa and only a marginal decrease versus film thickness. The SiC on Si(100) films show a substantially lower residual stresses, with highest values around 400 MPa for the thinnest films (60 nm) decreasing down to about 150 MPa for the 1 μm thick film. Note that the 20% higher elastic modulus of the SiC(111) films cannot account for such a different residual stress.

Interestingly, the Raman and the wafer curvature stress analyses are in reasonable agreement for the SiC on Si(100), confirming the Raman biaxial stress coefficient of $\Delta\omega_{TO} = 1125\ cm^{-1}$ as calibrated by Rohmfeld for 3C-SiC on Si(100). On the other hand, the same coefficient would lead to an overestimation of the biaxial stresses for the epitaxial films on Si(111). Our results suggest instead a higher coefficient around $\Delta\omega_{TO} \sim 1780\ cm^{-1}$ for the SiC on Si(111), as indicated by the average 900 MPa biaxial stress calculated from the wafer curvature measurements (Fig. 2) versus the observed average 4 cm^{-1} red Raman shift.

Since the expected strain from the thermal and lattice mismatches can be considered equivalent for growth on Si(100) and Si(111), the data discussed above indicate that biaxial stresses for 3C-SiC films grown on Si(100) surfaces relax in a very different way from films on Si(111) surfaces.

Films on Si(100) show a residual stress comparable to the expected thermal stress range, as a deposition temperature of 1000 °C and a coefficient of thermal expansion of $3.3 \times 10^{-6}\ K^{-1}$ for 3C-SiC[3] would lead to an extrinsic stress around 300 MPa. This also indicates that the intrinsic stress

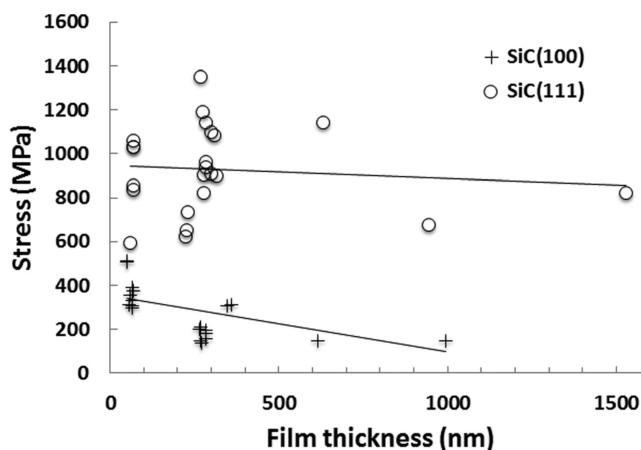

FIG. 2. Residual stress as estimated from wafer curvature measurements for epitaxial 3C-SiC films grown on Si(100) and Si(111) substrates. Films on Si(111) retain a much higher residual tensile stress showing only a marginal decrease versus film thickness. Inversely, films on Si(100) show substantially lower stress and the data trends indicate a clear decrease versus thickness.

originated from the 3C-SiC/Si lattice mismatch is essentially relaxed in SiC films on Si(100). Films grown on Si(111) store considerably more tensile stress, retaining, thus, still some fraction of the intrinsic stress component.

Moreover, the already low stresses of films on Si(100) tend to decrease further with thickness, whereas the biaxial stresses of the SiC films on Si(111) appear almost locked-in as shown in Fig. 2. The decrease of residual stress observed for thicker films on Si(100) is attributed to the time-dependent creep mechanism upon film growth, i.e., the evolution of defects such as stacking faults (SFs) and other types of dislocations. Such relaxation was reported to be more related to the total duration of the film growth than to the actual total film thickness.[10] However, Fig. 2 indicates that this decrease trend takes place at a much slower rate for films on Si(111).

XRD and LEED analysis confirmed, as commonly reported, that epitaxial mono-crystalline 3C-SiC films grow with ⟨100⟩ orientation on Si(100) and with ⟨111⟩ orientation on Si(111) surfaces (not shown).[1,23] This also means that the carbonisation layer in both cases is thin enough to maintain a coherent epitaxial relationship. The TEM micrographs of SiC on Si(100) (Fig. 3(a)) and on Si(111) (Fig. 3(b)) show in both cases a high density of Shockley-type SFs, which is the dominating stress relief mechanism for 3C-SiC films on silicon, due to their low formation energy.[24] It is not straightforward to quantify the amount of SFs in 3C-SiC on Si from TEM micrographs, due to their extremely high density.[25] However, while along the 300 nm thickness of the film grown onto the (100) surface (Fig. 3(a)) there is a substantial decrease in SF density, these stacking faults are not attenuated through the 300 nm 3C-SiC films on Si(111) (Fig. 3(b)). AFM contact topography substantiates these TEM observations with a visually rougher surface of the SiC films on Si(111) (Fig. 3(d)) compared to the same thickness films on Si(100) (Fig. 3(c)). A very high density of SFs is evident on the SiC(111) surface, which appears as fine ridges arranged in a 3-fold symmetry texture. Surface roughness analysis also confirms these observation with RMS values of 2.23 nm versus 3.45 nm for SiC(100) and SiC(111), respectively.

There is a fundamental geometrical difference between SFs in a 3C-SiC film growing along the ⟨111⟩ orientation as compared to a film oriented along ⟨100⟩. In the first case, the stacking faults are inclined about 55° with respect to their growth surface (100), corresponding to the angle between the {100} and {111} planes,[25] i.e., we are in the presence of SF along the {111} slip planes, or SF(111).

The stacking faults in the SiC films on Si(111) direction appear inclined about 70°, corresponding to the angle between the {111} and {−111} planes.[25] In fact, as SF(111) cannot give any strain relief in SiC films oriented in the ⟨111⟩ direction on Si(111), SF(−111) are created instead. However, as the inclination of SF(−111) onto the Si(111) growth surface is steeper than for the SF(111) onto the Si(100) surface (∼70° versus ∼55°, respectively), there are two important consequences. First, the SFs annihilation mechanism by which two stacking faults intersecting each other are eliminated by unfaulting reaction[26] is far less favourable. Additionally, a steeper SF inclination with respect to the growth plane (the plane where the film biaxial strain is located) will geometrically be less efficient for

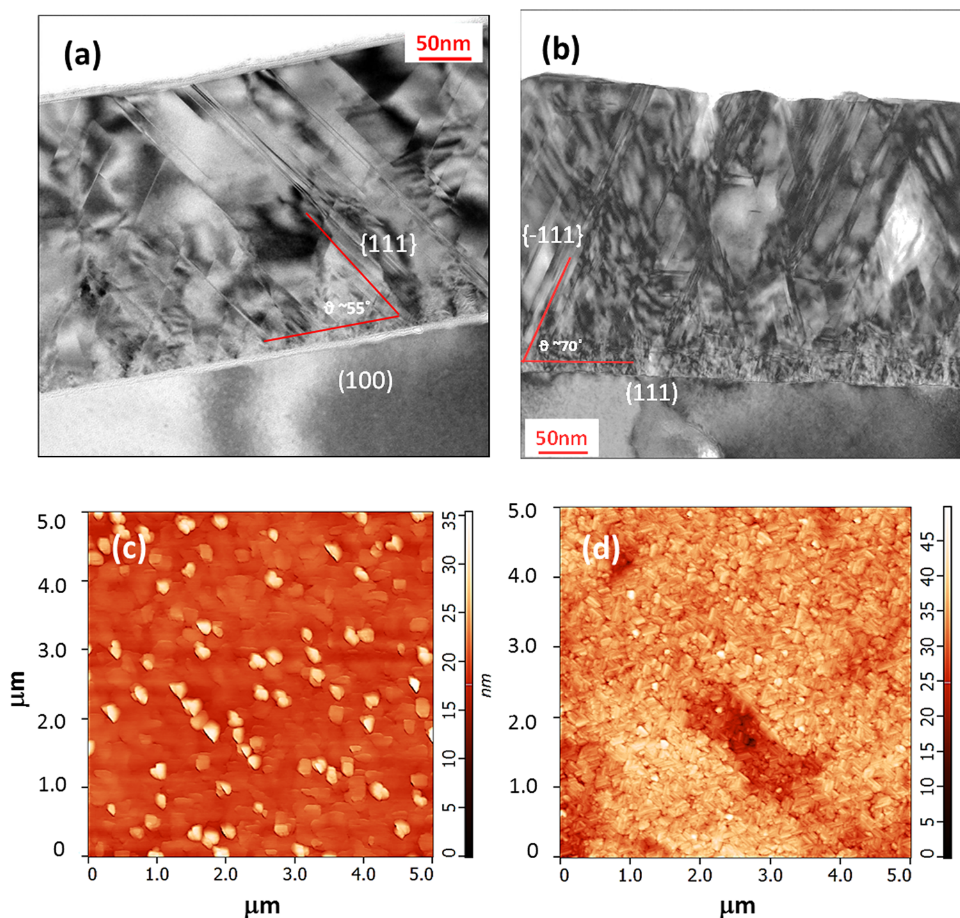

FIG. 3. TEM micrographs of 300 nm thick epitaxial 3C-SiC films on (a) SiC(100) and (b) Si(111), showing a 55° and 70° inclination, respectively, of SF over their growth planes. Note that the interface between the SiC and Si(100) in (a) was contaminated by glue during samples preparation. The AFM images in (c) and (d) show the corresponding surfaces of the SiC(100) and SiC(111) films, respectively.

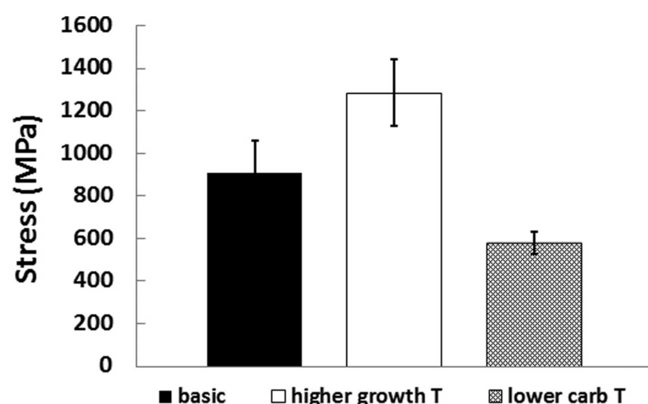

FIG. 4. Average stresses of 300 nm thick SiC(111) films grown (1) with the basic process of Fig. 1, (2) with a 1050 °C growth temperature (higher growth T), (3) with a 750 °C carbonisation temperature (lower carb T). Residual stresses increase with increasing temperatures involved in the growth process.

intrinsic strain relief. A rough 2D estimate of this effect is given by comparing the projections of the SF planes onto the growth plane for both cases, which are proportional to cosθ, with θ equal to 55° and 70° for SiC on Si(100) and Si(111), respectively (Fig. 3). As cos(70)/cos(55) $\sim$ 0.6, SF(111) in the SiC(100) films are expected to be roughly 40% more efficient in relieving the residual biaxial stress than SF($-$111) in the SiC(111) films. As a result, either a higher amount and/or thicker stacking faults will be required to achieve the same amount of strain relaxation for a SiC oriented along the $\langle 111\rangle$ direction than for a SiC film along the $\langle 100\rangle$ direction, and such that stacking faults will also persist longer versus films thickness for the SiC(111) films.

Finally, Fig. 4 indicates that the residual stresses in the SiC(111) films can be tuned within a large range by modifying the process temperatures of the epitaxial growth process steps. The graph bars compare average stresses for 300 nm SiC(111) films using the basic process in Fig. 2, to stresses from a slightly higher growth temperature (1050 °C) and from a lower carbonisation temperature (750 °C, as compared to 950 °C). An increase of 50 °C of the growth temperature leads to almost 50% increase in residual stress, whereas the lower carbonisation temperature leads to about a 50% decrease instead, as shown in Fig. 4. Note that we chose to lower the carbonisation rather than the growth temperature to ensure still comparable crystalline quality. Equivalent experiments with the SiC(100) films yielded a much smaller difference (below 20%), as the residual stress of the $\langle 100\rangle$ oriented films is more readily relaxed and typically left with the thermal component only.

In conclusion, thanks to a systematic study of stress behaviour of hetero-epitaxial 3C-SiC on silicon with Raman spectroscopy and wafer curvature monitoring, we can demonstrate that for equivalent growth conditions films grown along the $\langle 111\rangle$ direction on Si(111) tend to store considerably higher tensile residual stress than films grown along the $\langle 100\rangle$ orientation on Si(100). Moreover, as opposed to SiC(100)films, the high tensile residual stress of SiC(111) films only shows marginal decrease versus thickness.

We show that the 20% strain from the lattice mismatch of Si and 3C-SiC can be essentially relaxed for SiC(100) films as thin as 60 nm. On the other hand, the residual stress of 3C-SiC films on Si(111) retains a significant component of intrinsic stress. We explain this phenomenon through a higher strain relief efficiency of stacking faults in the SiC(100), which are less steeply inclined onto the growth plane of the epitaxial films.

This work, additionally to providing a fundamental insight in stress relief for highly mismatched hetero-epitaxy, shows that residual stresses in thin epitaxial 3C-SiC films on Si can be controlled within a broad tensile range (from a couple of hundreds of MPa up to over 1 GPa) by (1) selecting the appropriate substrate orientation, i.e., Si (100) for low stress versus Si(111) for high stress, and (2) fine-tuning the temperatures involved in the epitaxial process. This finding is highly valuable for MEMS applications, where the control of residual stresses of beams and diaphragm structures is crucial.[9]

The authors would like to acknowledge funding support from the Australian National Fabrication Facility, the Queensland State Government, and SPTS Technologies (San Jose, Ca). Dr. F. Iacopi is the recipient of an *Australian Research Council Future Fellowship* (FT120100445).

[1] S. Madapura, A. J. Steckl, and M. Loboda, J. Electrochem. Soc. **146**, 1197 (1999).
[2] H. Nagasawa and K. Yagi, Phys. Status Solidi B **202**, 335 (1997).
[3] V. Cimalla, J. Pezoldt, and O. Ambacher, J. Phys. D: Appl. Phys. **40**, 6386 (2007).
[4] C. A. Zorman and R. J. Parro, Phys. Status Solidi **245**, 1404 (2008).
[5] N. G. Wright, A. B. Horsfall, and K. Vassilevski, Mater. Today **11**, 16 (2008).
[6] S. Roy, C. Zorman, and M. Mehregany, J. Appl. Phys. **99**, 044108 (2006).
[7] H. Guckel, Sens. Actuators **28**, 133 (1991).
[8] A. A. Volinsky, G. Kravchenko, P. Waters, J. Deva Reddy, C. Locke, C. Frewin, and S. E. Saddow, Mater. Res. Soc. Symp. Proc. **1069**, D03-05 (2008).
[9] R. Anzalone, G. D'Arrigo, C. Locke, M. Camarda, S. E. Saddow, and F. La Via, J. Microelectromech. Syst. **20**, 745 (2011).
[10] M. Zielinski, A. Leycuras, S. Ndiaye, and T. Chassagne, Appl. Phys. Lett. **89**, 131906 (2006).
[11] S. Rohmfeld, M. Hundhausen, and L. Ley, Phys. Rev. B **58**, 9858 (1998).
[12] E. Bustarret, D. Vobornik, A. Roulot, T. Chassagne, G. Ferro, Y. Monteil, E. Martinez-Guerrero, H. Mariette, B. Daudin, and L. S. Dang, Phys. Status Solidi **195**, 18 (2003).
[13] I. De Wolf, Semicond. Sci. Technol. **11**, 139 (1996).
[14] S. Rohmfeld, M. Hundhausen, L. Ley, C. A. Zorman, and M. Mehregany, J. Appl. Phys. **91**, 1113 (2002).
[15] M. A. Capano, B. C. Kim, A. R. Smith, A. P. Kvam, S. Tsoi, and A. K. Ramdas, J. Appl. Phys. **100**, 083514 (2006).
[16] L. Wang, S. Dimitrijev, J. Han, P. Tanner, A. Iacopi, L. Hold, and B. H. Harrison, Thin Solid Films **519**, 6443 (2011).
[17] S. A. Kukushkin, A. V. Osipov, V. N. Bessolov, B. K. Medvedev, V. K. Nevolin, and K. A. Tcarik, Rev. Adv. Mater. Sci. **17**, 1 (2008).
[18] J. Komiyama, Y. Abe, S. Suzuki, and H. Nakanishi, Appl. Phys. Lett. **88**, 091901 (2006).
[19] E. G. Berasategui and T. F. Page, Surf. Coat. Technol. **163–164**, 491 (2003).
[20] K. Röll, J. Appl. Phys. **47**(7), 3224 (1976).
[21] See http://www.ioffe.ru/SVA/NSM/, Physical Properties of Semiconductors, electronic database, Ioffe Physical Technical Institute, St. Petersburg, Russia.
[22] T. Chassagne, G. Ferro, H. Haas, H. Mank, A. Leycuras, Y. Monteil, F. Soares, C. Balloud, Ph. Arcade, C. Blanc, H. Peyre, S. Juillaguet, and J. Camassel, Phys. Status Solidi **202**, 524 (2005).
[23] K. Shibahara, S. Nishino, and H. Matsunami, J. Cryst. Growth **78**, 538 (1986).
[24] U. Lindefelt, H. Iwata, S. Oberg, and P. R. Briddon, Phys. Rev. B **67**, 155204 (2003).
[25] A. Boulle, D. Chaussende, L. Latu-Romain, F. Conchon, O. Masson, and R. Guinebretière, Appl. Phys. Lett. **89**, 091902 (2006).
[26] Y. Hayafuji and S. Kawado, J. Appl. Phys. **53**, 1215 (1982).